FlatChem 15 (2019) 100108

Contents lists available at ScienceDirect

FlatChem

journal homepage: www.elsevier.com/locate/flatc

Exploiting the chemistry of redox active compounds to enhance the capacitance of reduced graphene oxide

P. Bharathidasan[a], Mustapha Balarabe Idris[a], Dong-Won Kim[b], S.R. Sivakkumar[a], S. Devaraj[a,*]

[a] Department of Chemistry, Centre for Energy Storage & Conversion, School of Chemical and Biotechnology, SASTRA Deemed University, Thanjavur 613401, India
[b] Department of Chemical Engineering, Hanyang University, Seoul 04763, Republic of Korea

ARTICLE INFO

Keywords:
Graphene
Improved capacitance
Redox active electrolyte
Redox couple
Reduced graphene oxide
Supercapacitor

ABSTRACT

The restacking of graphene sheets leading to poor electrical conductivity and reduced surface area strongly affects the capacitance properties of reduced graphene oxide (RGO). Many strategies employed to mitigate the restacking issue include the introduction of spacer materials between the graphene layers, hetero atom doping, compositing with metal oxides, etc. Herein, we report the enhancement of the capacitance properties of RGO by the addition of a small amount of redox active compounds, such as benzoquinone, KI, and NaI in the electrolyte. RGO is prepared by chemical exfoliation of graphite followed by a hydrothermal reduction in the presence of a small amount of hydrazine hydrate. The quality of prepared RGO is examined by microscopic and Raman spectroscopic studies. X-ray photoelectron spectroscopic studies reveal doping of 1.97 atomic weight % of nitrogen in RGO. The specific capacitance values of 105, 244, 322 and 414 F g^{-1} at a current density of 2 A g^{-1} are obtained for RGO in 0.25 M H_2SO_4 and 0.25 M H_2SO_4 containing 0.05 M of NaI, KI and benzoquinone, respectively. The enhancement in the specific capacitance of RGO is attributed to the reversible redox reaction of the additives. Interestingly, the mechanism of charge storage of RGO in NaI and KI containing electrolytes is different. Owing to rather slow kinetics of redox reaction of electrolyte additives, the rate performance of RGO has slightly compromised in redox active electrolytes.

1. Introduction

Graphene has been studied extensively as an electroactive material for supercapacitors because of its exciting properties such as high theoretical surface area (2630 $m^2 g^{-1}$), excellent conductivity, outstanding mechanical stability and high theoretical specific capacitance (550 F g^{-1}) [1–3]. However, production of high quality, optically transparent, single-layered graphene even in a small scale (few grams) is still challenging. Hence, research community focuses on synthesizing few-layered graphene by chemical methods. Among various chemical methods of preparation of few-layered graphene, Hummers' method is the most efficient [4]. Typically, few-layered graphene is prepared by oxidation of graphite followed by exfoliation of graphite oxide and subsequent reduction of graphene oxide. The few-layered graphene thus prepared is known as reduced graphene oxide (RGO) [5].

The major drawbacks of chemically synthesized RGO are (i) reduced electrical conductivity and (ii) low specific surface area, which in turn affect the capacitance properties [6]. Reduced electrical conductivity mainly arises from the presence of residual (unreduced) oxygen-based functionalities, whereas, van der Waals forces acting between the graphene sheets cause the agglomeration of sheets and consequently lead to the low specific surface area [7]. To mitigate these issues, several efforts have been devoted with the sole aim of improving the capacitance properties of RGO, which include, the introduction of spacers between the graphene sheets, hetero atom doping, compositing with metal oxides or conducting polymers [8–14], etc. Besides these, the capacitance properties of RGO can also be improved by the addition of redox couples in the electrolyte [15]. This strategy has been successfully adopted to improve the capacitance properties of activated carbon. Although this is a facile strategy and has huge potential, there are only very few reports on the usage of redox additive in the electrolyte to improve the capacitive storage performance of RGO [16–19]. For instance, Sankar and Selvan [16] have studied the effect of concentration of redox additive, KI on the capacitance properties of RGO. G K Veerasubramani et al. [17] have used sodium molybdate to improve the capacitance performance of flexible supercapacitor fabricated using RGO. Herein, the redox reactions of iodide/triiodide and quinone/hydroquinone are exploited to improve the capacitance properties of RGO. Also, the charge storage mechanism of RGO in redox active electrolytes is reported.

* Corresponding author.
E-mail address: devaraj@scbt.sastra.edu (S. Devaraj).

https://doi.org/10.1016/j.flatc.2019.100108
Received 12 November 2018; Received in revised form 12 April 2019; Accepted 24 April 2019
Available online 25 April 2019

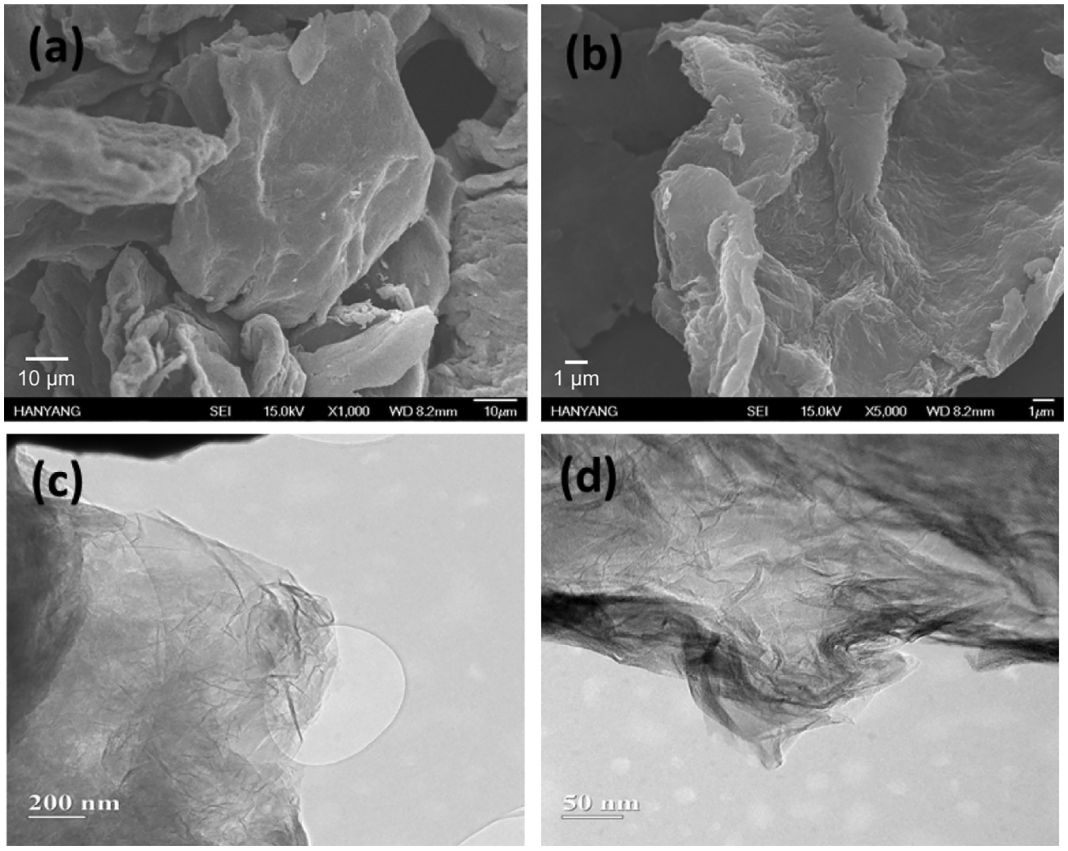

Fig. 1. (a, b) SEM and (c, d) TEM images of RGO.

2. Experimental

All the chemicals used in the present study were purchased from Sigma-Aldrich and Merck.

Graphene oxide (GO) was synthesized by modified Hummers' method [4]. In brief, 1 g of graphite was oxidized using 3 g of potassium permanganate and 0.5 g of sodium nitrate in an acidic medium (24 mL of con. H_2SO_4) at 5 °C. To this pasty mixture, 100 mL of double distilled (DD) water was added drop by drop. During the slow addition of DD water, the temperature of the mixture was increased suddenly to 90 °C, which was then allowed to attain room temperature naturally. Subsequently, 10 mL of 30% H_2O_2 was added to terminate the reaction. Thus obtained graphite oxide was washed several times with 1 M HCl and DD water consecutively until the pH became close to neutral. The washed colloidal dispersion was sonicated for 2 h to get clear dispersion of graphene oxide (GO). Subsequently, the exfoliated GO was separated by centrifuging the suspension at a high speed of 14,000 rpm and then it was vacuum dried at 60 °C for 12 h.

The as-prepared GO was reduced hydrothermally using hydrazine hydrate as a reducing agent. Typically, 60 mL of DD water was added to 160 mg of GO and subjected to sonication until the clear dispersion of GO was obtained. Subsequently, 18 μL of hydrazine hydrate was added, and the content was maintained at 180 °C for 12 h in Teflon lined stainless steel autoclave. The obtained black coloured product was washed with DD water followed by ethanol and then dried under vacuum at 60 °C.

The morphology of the as-synthesized RGO was studied using FEI scanning electron microscope, PHILIPS, XL30 SFEG, and transmission electron microscope, JEOL, JEM 2100F. Raman spectrum of RGO was recorded using Raman spectrophotometer, i Raman Plus, B&W TEK, USA, in which, a green laser (wavelength of 532 nm) served as an excitation source. The elemental composition of RGO was examined using X-ray photoelectron spectrophotometer (Thermo Scientific K-Alpha, USA) using monochromatized Al Kα as a source. All the X-ray photoelectron spectra were calibrated against adventitious carbon (C 1s binding energy, 284.6 eV) and analyzed using XPSPEAK 41 software. A Shirley-type background was subtracted from the recorded spectra and then curve fitting was carried out with a combination of Gaussian and Lorentzian curves (Voigt type) after adding required number of p-type sub-peaks. The fitting was carried out until χ^2 value of < 1 was obtained. The derived binding energies are accurate to ± 0.1 eV. The N_2 sorption isotherm was recorded at 77 K using accelerated surface area and porosimetry system, Autosorb-iQ station 2. Prior to surface area measurements, RGO was degassed at 120 °C for 12 h under vacuum.

To study the capacitance properties, composite electrodes of RGO were prepared by manually casting the slurry on both sides of high purity stainless steel (SS) foil. The slurry was prepared by mixing RGO with a conductive carbon (carbon black, super P) and a binder (polyvinylidene fluoride) in the weight ratio of 7:2:1 followed by addition of a few drops of 1-methyl-2-pyrrolidone. The cast electrodes were vacuum dried at 110 °C for 8 h prior to the capacitance measurements. The capacitance properties of the composite electrodes were studied in 0.25 M H_2SO_4 (pristine electrolyte) and redox active electrolytes (0.25 M H_2SO_4 containing 0.05 M of NaI or KI or benzoquinone). The cyclic voltammograms and galvanostatic charge-discharge cycling were recorded between 0 and 0.8 V vs Ag/AgCl. Electrochemical impedance spectra (EIS) were recorded in the frequency range of 100 kHz to 100 mHz by exciting the cell with a sinusoidal voltage of 10 mV amplitude at a DC potential of 0.4 V. EIS were fitted using software, Z Fit and an appropriate equivalent circuit was generated. All the electrochemical measurements were performed using potentiostat/galvanostat, Biologic SP-200 in a three-electrode configuration.

3. Result and discussion

The formation of few-layered graphene is observed from the SEM

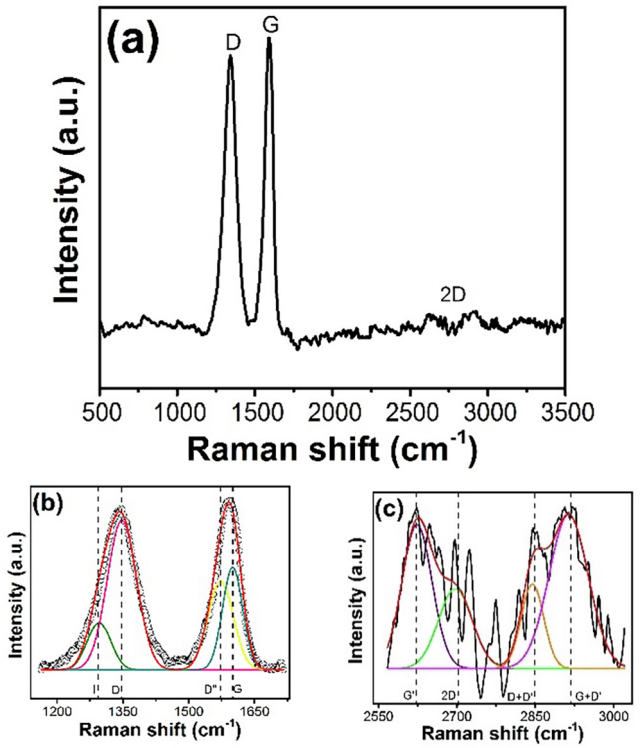

Fig. 2. (a) Raman spectrum and (b,c) deconvoluted Raman spectra of RGO.

images (Fig. 1a, b) of RGO. The TEM images of RGO (Fig. 1c, d) confirm the formation of large, thin sheets of few-layered graphene. Owing to aggressiveness of the chemicals used for the synthesis of RGO, wrinkling is observed at the edge of sheets. Raman spectrum of single-layered graphene is expected to show characteristic G and 2D bands with an I_{2D}/I_G ratio of ~2 [20,21]. However, owing to the introduction of defects/disorders, few-layered graphene synthesized by chemical exfoliation method, as in the present case, exhibits disordered or defective band (D band) besides G and 2D bands (Fig. 2a). The observed shift in the position of G band is an indication of nitrogen doping in RGO [22]. Further, the very low value of I_{2D}/I_G (0.071) obtained for as-synthesized RGO after deconvolution of D, G and 2D bands (Fig. 2b and C) suggests multiple layers of graphene (more than five layers) [21].

To further confirm the nitrogen doping in RGO and to quantify the different types of nitrogen, X-ray photoelectron spectrum was recorded and analyzed. The survey spectrum of RGO (Fig. 3a) exhibits peaks corresponding to carbon, nitrogen, and oxygen only. While unreduced oxygen-based functionalities exhibit peak for oxygen, the observed peak for nitrogen confirms doping of nitrogen in RGO. As given in Table 1, 1.97 atomic weight % of nitrogen is found in RGO. Further, deconvolution of core level C1s spectrum of RGO (Fig. 3b) shows the presence of four different types of carbon (C−C/C═C, C−N, C−O and C═O), whereas, two different types of oxygen (C═O and COO^-) are found in the deconvoluted core level O1s spectrum of RGO [23,24]. The core level N1s spectrum of RGO (Fig. 3d) is deconvoluted into four subpeaks corresponding to four different types of nitrogen, namely, pyridinic (16.49%), pyrrolic (15.23%), quaternary (37.92%), pyridinic oxide (30.36%) and their relative proportion is shown in Fig. 4. As reported in the literature, doping of pyridinic and pyrrolic type nitrogen in RGO is advantageous since they can contribute to the capacitance of RGO via Faradaic reactions [25]. Also, quaternary nitrogen, as the major contributor, is expected to improve the electrical conductivity of RGO [26–28].

The nitrogen adsorption-desorption isotherm of RGO (Fig. 5a) demonstrates type IV behaviour with very wide H2 type hysteresis loop (relative pressure (P/P_o) range of 0.23 to 0.93), indicating mesoporous characteristics of the RGO with a large number of mesopores. The Brunauer-Emmett-Teller (BET) surface area, which accounts for all types of pores (micro, meso, and macropores), is high (376 $m^2\ g^{-1}$). However, there is a substantial contribution from the micropores as inferred from the steep increase in the volume of nitrogen adsorbed at very low relative pressure. Since micropores are not very suitable for charge storage [29], BJH surface area, which takes account of only mesopores, is calculated and it is also high (289 $m^2\ g^{-1}$). The single point pore volume is found to be 0.312 $cm^3\ g^{-1}$. The BJH pore size distribution obtained from the desorption branch of the isotherm (Fig. 5b) is narrow with a peak at 3.840 nm, which confirms ordered mesoporosity in RGO. The high surface area and large pore volume, in addition to the presence of uniform mesopores, would provide more active sites for charge storage and decrease the diffusion path of ions, resulting in high utilization of the active material [30].

The cyclic voltammogram (CV) of RGO recorded in an aqueous 0.25 M H_2SO_4 electrolyte (Fig. 6a) shows nearly rectangular shape with a small deviation at around 0.3 V. This observed deviation from the rectangular shape is attributed to the Faradaic reaction of doped pyrrolic and pyridinic nitrogen of RGO. Upon addition of a small amount of benzoquinone corresponding to 0.05 M into aqueous 0.25 M H_2SO_4 electrolyte (H_2SO_4-Q), an anodic and a cathodic redox peak is observed at 0.380 and 0.171 V, respectively. The benzoquinone turned into hydroquinone as soon as it was added into pristine H_2SO_4 electrolyte [31], and the hydroquinone formed undergoes oxidation to benzoquinone during charging (forward scan) and reduces to hydroquinone during discharging (reverse scan) corresponding to transfer of two electrons as shown in equation (1). Owing to this redox reaction, the area under the CV of RGO recorded in H_2SO_4-Q electrolyte is larger than that in the pristine H_2SO_4 electrolyte, indicating higher specific capacitance for RGO in H_2SO_4-Q electrolyte than in pristine H_2SO_4 electrolyte.

(1)

The charge-discharge cycles of RGO were recorded in pristine H_2SO_4, and H_2SO_4-Q electrolytes at various current densities and typical charge-discharge curves recorded at a current density of 2 A g^{-1} are shown in Fig. 6b. While the potential of RGO increases/decreases linearly during charging/discharging in the pristine H_2SO_4 electrolyte, plateaus centred around 0.3 V is observed in the charge-discharge cycle of RGO recorded in H_2SO_4-Q electrolyte. Since charge-discharge profile of RGO in H_2SO_4-Q electrolyte is non-linear, the specific energy and the specific capacitance values are calculated using the following equations [32].

$$\text{Specific energy}\,(E_{sp}) = \text{area under the discharge curve}/\Delta m \cdot 3.6 \quad (2)$$

As shown in the equation (3), area under the discharge curve is obtained by integrating the discharge curve with respect to time.

$$\text{area under the discharge curve} = I \int_{(U_{max})}^{(U_{min})} U\ (t)dt \quad (3)$$

where I is the current (A), U is the potential (V) and Δm is mass of the electroactive material (g). The corresponding specific capacitance is calculated using the following equation:

$$\text{specific capacitance} = 2E_{sp}/U_{max}^2 \quad (4)$$

Accordingly, a specific capacitance of 414 F g^{-1} obtained at a current density of 2 A g^{-1} for RGO in H_2SO_4-Q electrolyte is almost four times the specific capacitance obtained for RGO in the pristine H_2SO_4 electrolyte (105 F g^{-1}). This is attributed to the redox chemistry of benzoquinone (equation (1)). The variation of specific capacitance of RGO as a function of discharge current density in both the electrolytes is shown in Fig. 6c. While RGO retains 65.71% of its initial specific capacitance value in pristine H_2SO_4 electrolyte, retention of only 51.4%

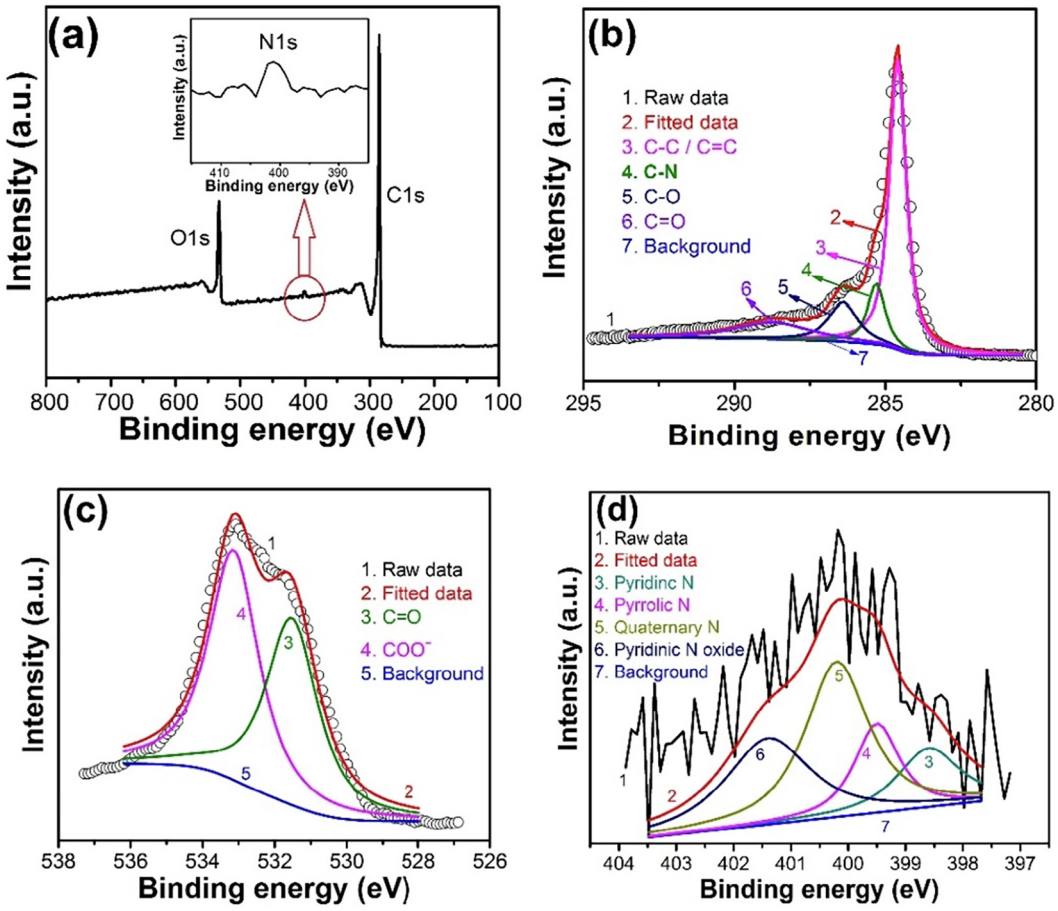

Fig. 3. (a) Survey and deconvoluted core level C1s (b), O1s (c) and N1s (d) X-ray photoelectron spectra of RGO.

Table 1
Elemental composition of RGO.

Element	Peak position (eV)	Relative atomic weight %
Carbon	284.62	86.02
Nitrogen	400.20	1.97
Oxygen	532.70	12.01

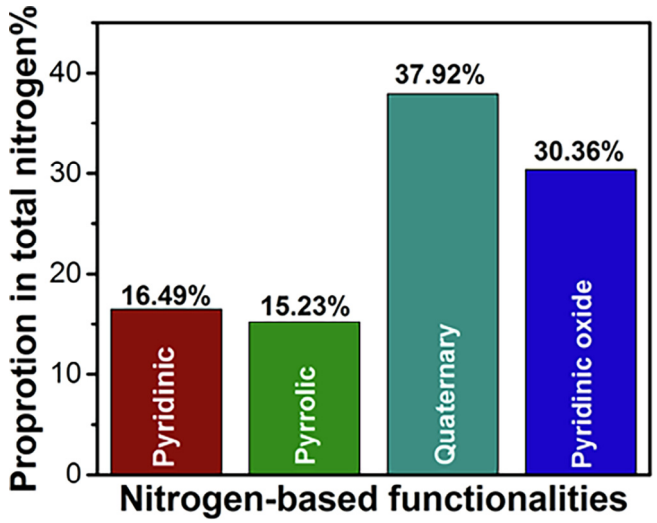

Fig. 4. The proportion of various nitrogen-based functionalities present in RGO.

of initial specific capacitance value of RGO is witnessed in H_2SO_4-Q electrolyte, which is attributed to the combined effect of reduction in the conductivity of the electrolyte on the addition of benzoquinone (Table 2) and inherent slow reaction kinetics of benzoquinone/hydroquinone transformation [31].

The CV of RGO recorded in the pristine H_2SO_4 electrolyte, 0.25 M H_2SO_4 containing 0.05 M NaI (H_2SO_4-NaI) and 0.25 M H_2SO_4 containing 0.05 M KI (H_2SO_4-KI) are shown in Fig. 7. As discussed earlier, due to the Faradaic reaction of doped pyrrolic and pyridinic nitrogen, the CV of RGO recorded in pristine H_2SO_4 electrolyte shows a potential-dependent change in the voltammetric current below 0.4 V and potential independent stable voltammetric current above 0.4 V due to adsorption/desorption of ions at the electrode/electrolyte interface. Addition of redox active compounds, NaI or KI into pristine H_2SO_4 electrolyte results in the appearance of reversible redox peaks. The charge associated with the CV curves of RGO follows this order: H_2SO_4-KI > H_2SO_4-NaI > pristine H_2SO_4 electrolyte, indicating the highest specific capacitance for RGO in H_2SO_4-KI electrolyte. It has been reported that the following redox reactions (equations (5) to (8)) are possibly responsible for the observed redox peaks in the H_2SO_4-KI electrolyte [16].

$$3I^- \leftrightarrow I_3^- + 2e^- \quad (5)$$

$$2I^- \leftrightarrow I_2 + 2e^- \quad (6)$$

$$2\,I_3^- \leftrightarrow 3I_2 + 2e^- \quad (7)$$

$$I_2 + 6H_2O \leftrightarrow 2IO_3^- + 12H^+ + 10e^- \quad (8)$$

To understand the mechanism of charge storage in RGO due to the redox chemistry of NaI and KI, UV–visible spectra were recorded at various states of charge (SoC) and are shown in Fig. 7b and c. The

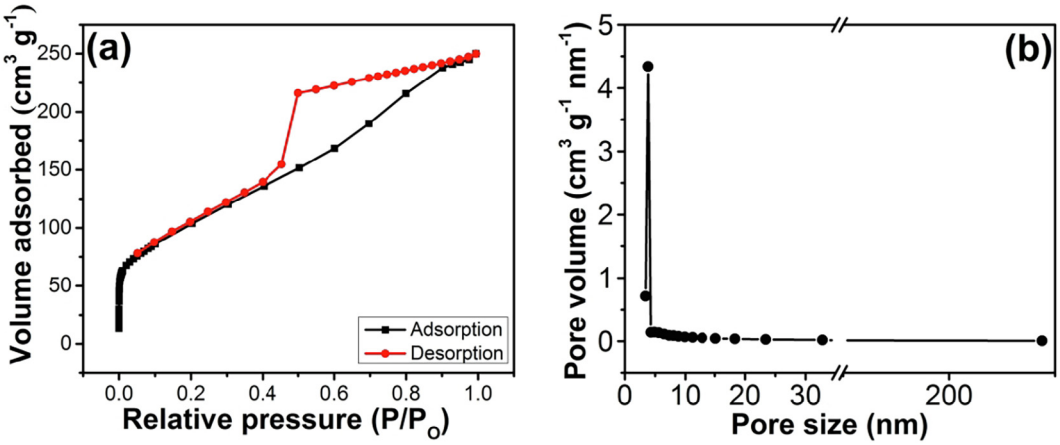

Fig. 5. (a) Nitrogen adsorption-desorption isotherm and (b) corresponding BJH pore size distribution of RGO.

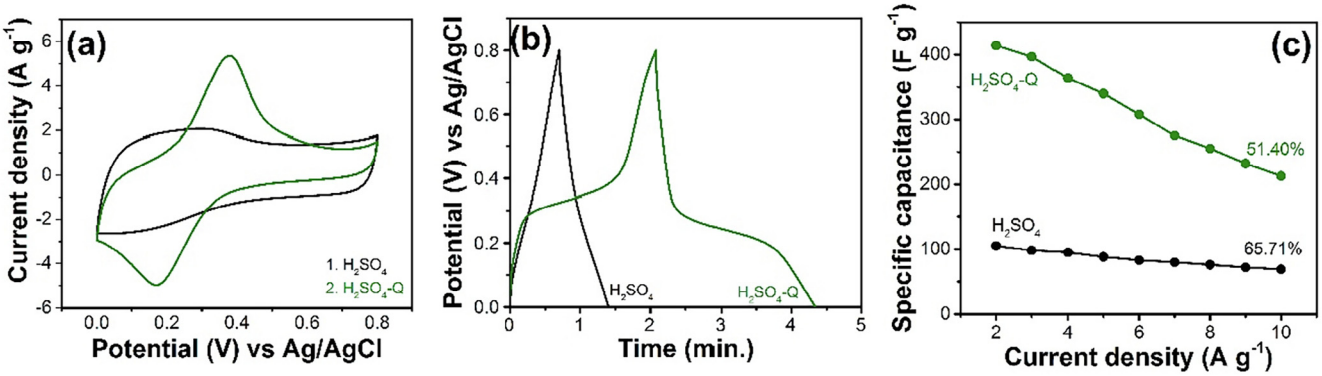

Fig. 6. (a) Cyclic voltammograms of RGO recorded at a sweep rate of 20 mV s^{-1}, (b) charge-discharge cycles of RGO recorded at a current density of 2 A g^{-1} and (c) rate performance of RGO in 0.25 M H_2SO_4 and 0.25 M H_2SO_4 electrolyte containing 0.05 M of benzoquinone.

Table 2
The ionic conductivity of pristine electrolyte (0.25 M H_2SO_4) and 0.25 M H_2SO_4 containing 0.05 M NaI (H_2SO_4-NaI), 0.05 M KI (H_2SO_4-KI), 0.05 M benzoquinone (H_2SO_4-Q).

S. No.	Electrolyte	Ionic conductivity (mS cm^{-1})
1	Pristine H_2SO_4	100.1
2	H_2SO_4-NaI	113.2
3	H_2SO_4-KI	128.7
4	H_2SO_4-Q	97.0

UV–visible spectra of H_2SO_4-NaI (Fig. 7b) and H_2SO_4-KI (Fig. 7c) electrolytes recorded at open circuit potential exhibit only one peak corresponding to iodide ions, suggesting the presence of iodide ions in the electrolyte on the addition of either NaI or KI into pristine H_2SO_4 electrolyte [33–35]. The UV–visible spectra of both electrolytes (H_2SO_4-NaI and H_2SO_4-KI) recorded after charging the electrode to SoC of 100% show characteristic peaks corresponding to triiodide ions, which disappear on discharging the electrode completely to SoC of 0% [35]. However, in the case of H_2SO_4-NaI electrolyte, a less intense peak corresponding to iodine (inset of Fig. 7b) is also observed at SoC of 100% [35]. Thus, the mechanism of charge storage of RGO in H_2SO_4-KI electrolyte is shuttling of iodide and triiodide ions during charging and discharging processes as given in the equation (5). Besides, shuttling of iodide and triiodide ions during charging and discharging processes, the conversion of iodide ions into iodine and back to iodide ions (equation (6)) also contribute to the charge storage of RGO in H_2SO_4-NaI electrolyte. Further, it can also be inferred from Fig. 7b and c that the intensity of peaks corresponding to triiodide ions is higher for H_2SO_4-KI electrolyte than for H_2SO_4-NaI electrolyte suggesting that the conversion of iodide ions into triiodide ions is more feasible in H_2SO_4-KI electrolyte than H_2SO_4-NaI electrolyte.

To understand further, CVs of RGO were recorded at various sweep rates in both H_2SO_4-NaI and H_2SO_4-KI electrolytes and are presented in Figs. 8a and 9a, respectively. As it can be seen, on increasing the sweep rate, there is an increase in anodic (I_{pa}), cathodic (I_{pc}) peak currents and an increase in the peak potential difference (ΔE_p). The anodic and cathodic peak current values from the CVs recorded at various sweep rates were plotted against the square root of sweep rate and it was fitted to a straight line (Figs. 8b,c, and 9b,c). Both anodic and cathodic peak current values exhibit near linear variation with the square root of sweep rate, which suggests that the redox reactions are diffusion-controlled following Randles-Ševčík equation (9).

$$I_p = -2.69 \times 10^5 A\, C\, n^{3/2} D^{1/2} \nu^{1/2} \quad (9)$$

where A is an area of the electrode, C is a concentration of the active species, n is a number of electrons involved in the reaction, D is diffusion coefficient of the active species, and ν is sweep rate. The observed slight deviation from the linear variation of peak currents with the square root of sweep rate is due to the poor reaction kinetics of redox active compounds (NaI and KI) at higher sweep rates. From the slope of the linear plot, the diffusion coefficient was determined using equation (9). The diffusion coefficients calculated from the slope of the Figs. 8b and 9b using Randles-Ševčík equation are 4.08×10^{-6} and 3.38×10^{-5} cm^2 s^{-1}, for H_2SO_4-NaI and H_2SO_4-KI, respectively. The observed higher diffusion coefficient for H_2SO_4-KI than for H_2SO_4-NaI electrolyte is indicative of higher conversion of iodide ions into triiodide ions in H_2SO_4-KI than in H_2SO_4-NaI electrolyte.

Galvanostatic charge-discharge cycles of RGO recorded in pristine H_2SO_4, H_2SO_4-NaI and H_2SO_4-KI electrolytes are presented in Fig. 10a.

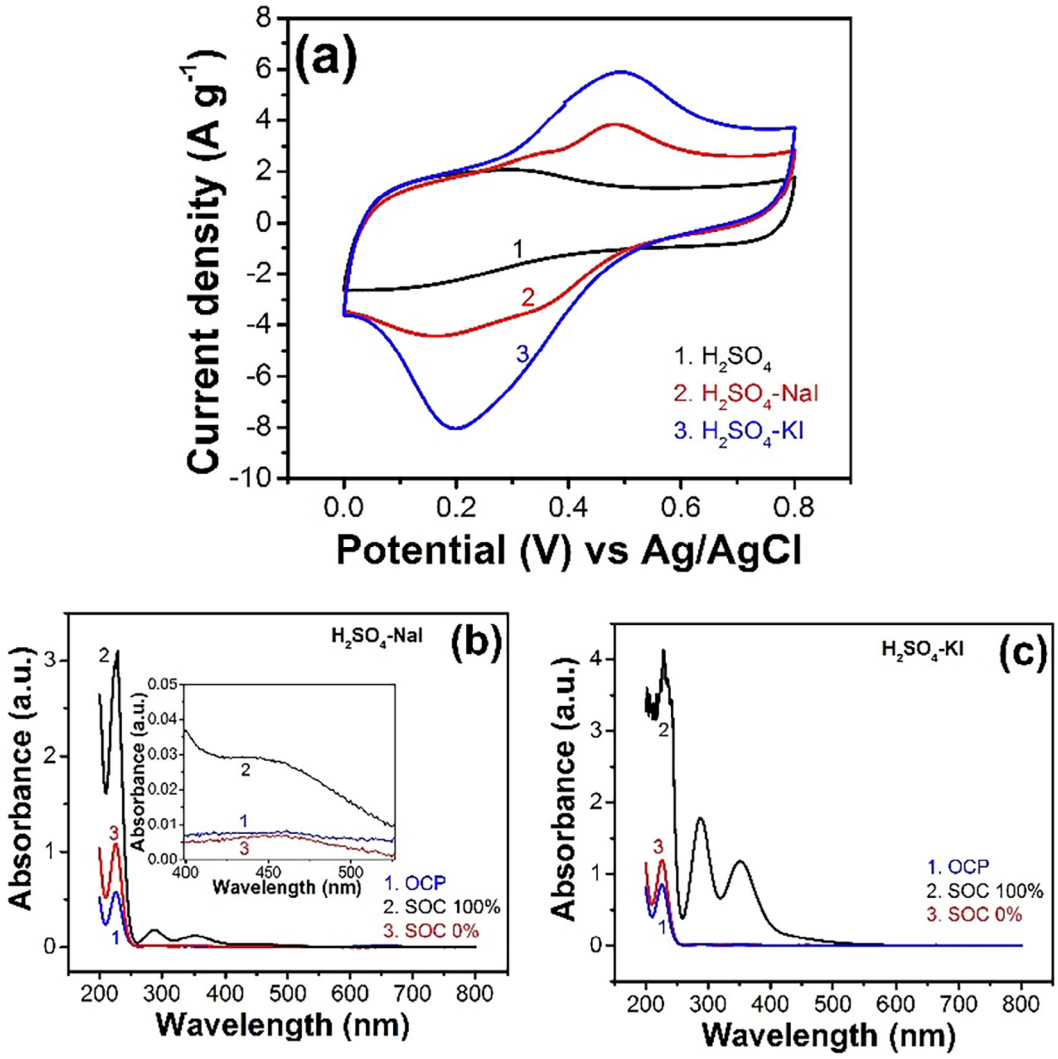

Fig. 7. (a) Cyclic voltammograms of RGO recorded at a sweep rate of 20 mV s^{-1} in pristine H_2SO_4, H_2SO_4-NaI and H_2SO_4-KI electrolytes. UV–Visible spectra of (b) H_2SO_4-NaI and (c) H_2SO_4-KI electrolytes recorded at various states of charge. Enlarged view of UV–Visible spectra (400–600 nm) of H_2SO_4-NaI electrolyte at various states of charge is given as inset in Fig. 7b.

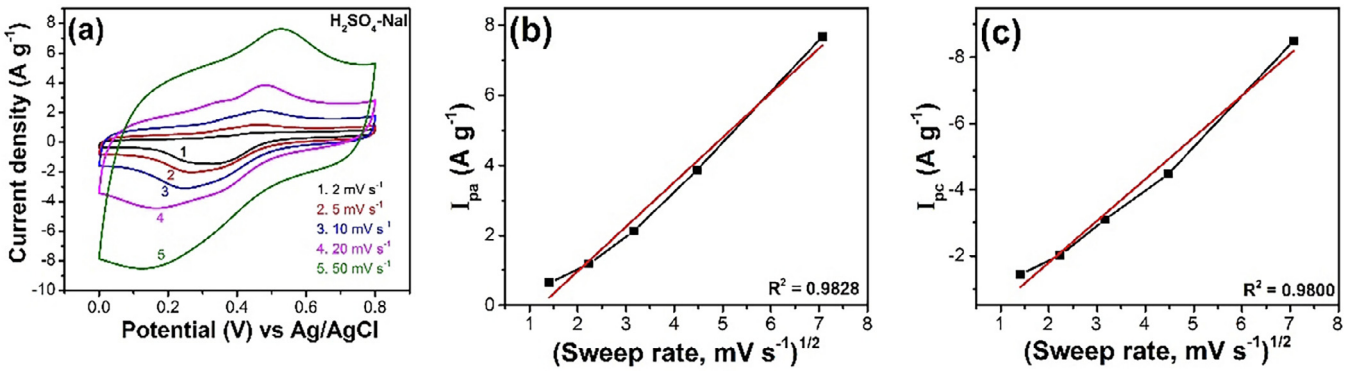

Fig. 8. (a) Cyclic voltammograms of RGO recorded at various sweep rates in H_2SO_4-NaI electrolyte, a variation of anodic peak current (b) and cathodic peak current (c) as a function of square root of sweep rate.

As mentioned earlier, the charge-discharge profile of RGO in pristine H_2SO_4 electrolyte exhibits a linear increase and decrease in the potential during charging and discharging, respectively with a small deviation around 0.3 V. Owing to shuttling of iodide and triiodide ions in the H_2SO_4-KI electrolyte, clear plateaus are observed in the charge-discharge profile of RGO. Though there is shuttling of iodide ions into iodine in addition to shuttling of iodide and triiodide ions, only a small deviation from the linear variation of potential with time is observed in the charge-discharge curve of RGO recorded in H_2SO_4-NaI electrolyte, which can be ascribed to lower conductivity of H_2SO_4-NaI electrolyte than H_2SO_4-KI electrolyte (Table 2) and inherent poor ionic conductivity of iodine formed during charging. The specific capacitance of

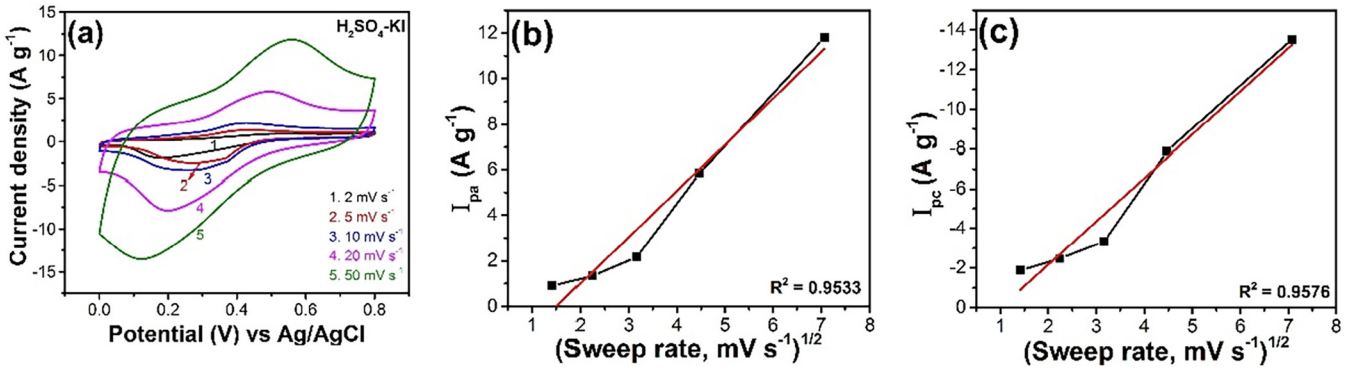

Fig. 9. (a) Cyclic voltammograms of RGO recorded at various sweep rates in H_2SO_4-KI electrolyte, a variation of anodic peak current (b) and cathodic peak current (c) as a function of square root of sweep rate.

RGO calculated from the charge-discharge curves recorded at a current density of $2\,A\,g^{-1}$ following Laheäär et al.'s recommendation [35] follows the order: H_2SO_4-KI ($322\,F\,g^{-1}$) > H_2SO_4-NaI ($244\,F\,g^{-1}$) > pristine H_2SO_4 electrolyte ($105\,F\,g^{-1}$). Among three electrolytes, the highest specific capacitance obtained for RGO in H_2SO_4-KI electrolyte is attributed to (i) facile shuttling of iodide and triiodide ions and (ii) higher ionic conductivity of H_2SO_4-KI electrolyte (Table 2) than pristine and H_2SO_4-NaI electrolytes.

The variation of specific capacitance of RGO as a function of discharge current density in pristine H_2SO_4, H_2SO_4-NaI and H_2SO_4-KI electrolytes are shown in Fig. 10b. The retention in the specific capacitance of RGO when the current density is increased from 2 to $10\,A\,g^{-1}$ follows this order: pristine H_2SO_4 (65.71%) > H_2SO_4-KI (63.04%) > H_2SO_4-NaI (60.24%). A small decrease in the rate performance of RGO in redox active electrolytes (H_2SO_4-KI and H_2SO_4-NaI) is attributed to the sluggish kinetics of reactions (5) and (6). Owing to facile shuttling of iodide and triiodide ions than iodide ions and iodine, comparatively better rate performance is achieved for RGO in H_2SO_4-KI electrolyte than in H_2SO_4-NaI electrolyte.

To study the influence of redox additives on the self-discharge, RGO electrodes were charged to upper cutoff potential in all the electrolytes and variation of potential as a function of time was monitored for 5 h without connecting to load (Fig. 11). The potential of RGO electrode in pristine H_2SO_4 electrolyte drops from the upper cutoff potential to 0.45 V in about 30 min and then decays marginally. In the case of H_2SO_4-KI and H_2SO_4-NaI electrolytes, there is a loss of only 175 mV over a period of 5 h owing to higher ionic conductivity of H_2SO_4-KI and H_2SO_4-NaI electrolytes than pristine electrolyte (Table 2). However, the potential of RGO electrode in H_2SO_4-Q electrolyte drops drastically to 0.2 and 0.1 V in 30 and 60 min, respectively and then it stabilizes around 0.1 V. Though RGO exhibits highest specific capacitance in H_2SO_4-Q electrolyte, its rate performance and self-discharge are poor. This is attributed to decrease in the conducting of the electrolyte on addition of benzoquinone (Table 2).

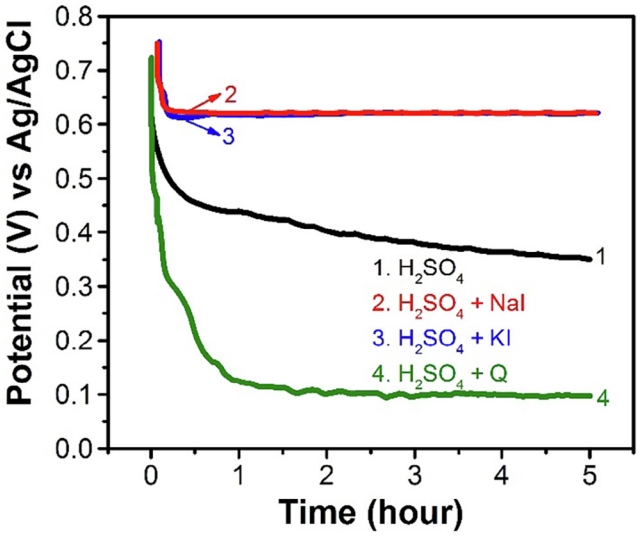

Fig. 11. Self-discharge profile of RGO recorded in pristine H_2SO_4, H_2SO_4-Q, H_2SO_4-NaI and H_2SO_4-KI electrolytes for a period of 5 h.

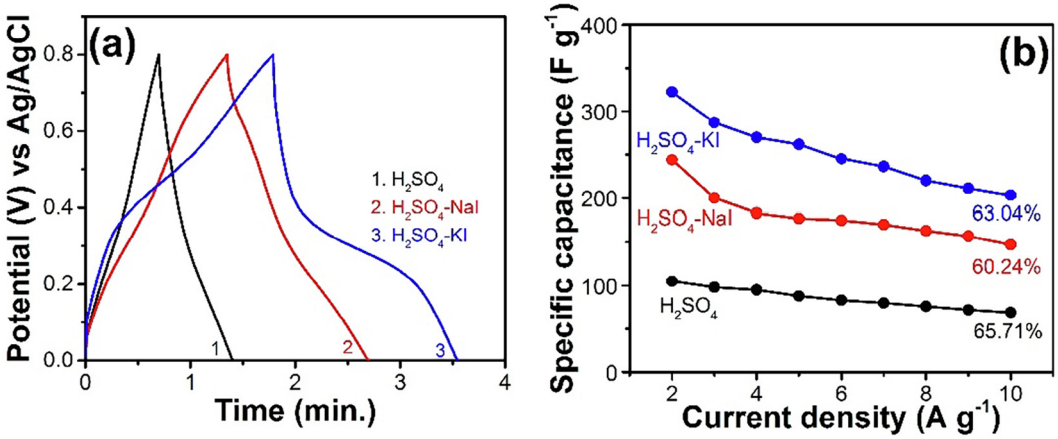

Fig. 10. (a) Charge-discharge cycle of RGO recorded at a current density of $2\,A\,g^{-1}$ and (b) variation of specific capacitance of RGO as a function of discharge current density in pristine H_2SO_4, H_2SO_4-NaI and H_2SO_4-KI electrolytes.

4. Conclusion

The redox chemistry of electrolyte additives such as benzoquinone, KI, and NaI are exploited to improve the capacitance properties of RGO. The specific capacitance values of 105, 244, 322 and 414 F g^{-1} are obtained at a current density of 2 A g^{-1} for RGO in pristine H_2SO_4, H_2SO_4-NaI, H_2SO_4-KI and H_2SO_4-Q electrolytes, respectively. The enhancement in the specific capacitance of RGO in H_2SO_4-Q electrolyte is attributed to the reversible redox reaction of quinone/hydroquinone. The mechanistic studies reveal that reversible conversion of iodide ions into triiodide ions contributes to the enhancement of the specific capacitance of RGO in H_2SO_4-KI electrolyte. Besides above referred reversible conversion of iodide ions into triiodide ions, reversible shuttling of iodide ions and iodine also contributes to the enhancement in the specific capacitance of RGO in H_2SO_4-NaI electrolyte. Hence, the addition of redox active compounds to the electrolyte is a facile strategy to improve the capacitance of RGO. However, owing to the comparatively slow kinetics of reversible redox reactions of the additives, the rate performance is slightly compromised.

Conflict of interest

There is no conflict of interests.

Acknowledgements

Financial support from Science and Engineering Research Board, Department of Science and Technology (SB/FT/CS-025/2014 & SB/FT/CS-070/2012) is gratefully acknowledged. We thank Dr. V. Ramanathan for Raman spectroscopic studies and SASTRA for infrastructural and instrumental facilities. One of the authors (PB) acknowledges CSIR, India for senior research fellowship and Mr. MBI acknowledges SASTRA for teaching assistantship.

Appendix A. Supplementary data

Supplementary data to this article can be found online at https://doi.org/10.1016/j.flatc.2019.100108.

References

[1] C. Lee, X. Wei, J.W. Kysar, J. Hone, Measurement of the elastic properties and intrinsic strength of monolayer graphene, Science 321 (2008) 385–388.
[2] A.S. Mayorov, R.V. Gorbachev, S.V. Morozov, L. Britnell, R. Jalil, L.A. Ponomarenko, P. Blake, K.S. Novoselov, K. Watanabe, T. Taniguchi, Micrometer-scale ballistic transport in encapsulated graphene at room temperature, Nano Lett. 11 (2011) 2396–2399.
[3] A.A. Balandin, Thermal properties of graphene and nanostructured carbon materials, Nat. Mater. 10 (2011) 569–581.
[4] W.S. Hummers Jr., R.E. Offeman, Preparation of graphitic oxide, J. Am. Chem. Soc. 80 (1958) 1339.
[5] D.R. Dreyer, S. Park, C.W. Bielawski, R.S. Ruoff, The chemistry of graphene oxide, Chem. Soc. Rev. 39 (2010) 228–240.
[6] K. Erickson, R. Erni, Z. Lee, N. Alem, W. Gannett, A. Zettl, Determination of the local chemical structure of graphene oxide and reduced graphene oxide, Adv. Mater. 22 (2010) 4467–4472.
[7] F. Wang, S. Xiao, Y. Hou, C. Hu, L. Liu, Y. Wu, Electrode materials for aqueous asymmetric supercapacitors, RSC Adv. 3 (2013) 13059–13084.
[8] P. Bharathidasan, D.-W. Kim, S. Devaraj, S.R. Sivakkumar, Supercapacitive characteristics of carbon-based graphene composites, Electrochim. Acta 204 (2016) 146–153.
[9] H. Jin, X. Wang, Z. Gu, Q. Fan, B. Luo, A facile method for preparing nitrogen-doped graphene and its application in supercapacitors, J. Power Sources 273 (2015) 1156–1162.
[10] M. Li, G. Sun, P. Yin, C. Ruan, K. Ai, Controlling the formation of rodlike V_2O_5 nanocrystals on reduced graphene oxide for high-performance supercapacitors, ACS Appl. Mater. Interfaces 5 (2013) 11462–11470.
[11] T. Kuilla, S. Bhadra, D. Yao, N.H. Kim, S. Bose, J.H. Lee, Recent advances in graphene based polymer composites, Prog. Polym. Sci. 35 (2010) 1350–1375.
[12] Y.B. Tan, J.M. Lee, Graphene for supercapacitor applications, J. Mater. Chem. A 1 (2013) 14814–14843.
[13] A.S. Lemine, M.M. Zagho, T.M. Altahtamouni, N. Bensalah, Graphene a promising electrode material for supercapacitors—a review, Int. J. Energy Res. 42 (2018) 4284–4300.
[14] Y. Huan, J. Liang, Y. Chen, An overview of the applications of graphene-based materials in supercapacitors, Small 8 (2012) 1805–1834.
[15] N.A. Kumar, H.-J. Choi, Y.R. Shin, D.W. Chang, L. Dai, J.-B. Baek, Polyaniline-grafted reduced graphene oxide for efficient electrochemical supercapacitors, ACS Nano 6 (2012) 1715–1723.
[16] K.V. Sankar, R.K. Selvan, Improved electrochemical performances of reduced graphene oxide based supercapacitor using redox additive electrolyte, Carbon 90 (2015) 260–273.
[17] G.K. Veerasubramani, K. Krishnamoorthy, P. Pazhamalai, S.J. Kim, Enhanced electrochemical performances of graphene based solid-state flexible cable type supercapacitor using redox mediated polymer gel electrolyte, Carbon 105 (2016) 638–648.
[18] T. Brousse, C. Cougnon, D. Bélanger, Grafting of quinones on carbons as active electrode materials in electrochemical capacitors, J. Braz. Chem. Soc. 29 (2018) 989–997.
[19] S. Yamazaki, T. Ito, M. Yamagata, M. Ishikawa, Non-aqueous electrochemical capacitor utilizing electrolytic redox reactions of bromide species in ionic liquid, Electrochim. Acta 86 (2012) 294–297.
[20] A.C. Ferrari, J.C. Meyer, V. Scardaci, C. Casiraghi, M. Lazzeri, F. Mauri, S. Piscanec, D. Jiang, K.S. Novoselov, S. Roth, A.K. Geim, Raman spectrum of graphene and graphene layers, Phys. Rev. Lett. 97 (2006) 187401.
[21] H.D. Le, T.T.T. Ngo, D.Q. Le, X.N. Nguyen, N.M. Phan, Synthesis of multi-layer graphene films on copper tape by atmospheric pressure chemical vapor deposition method, Adv. Nat. Sci-Nanosci. 4 (2013) 035012.
[22] Z. Zafar, Z.H. Ni, X. Wu, Z.X. Shi, H.Y. Nan, J. Bai, L.T. Sun, Evolution of Raman spectra in nitrogen doped graphene, Carbon 61 (2013) 57–62.
[23] J.R. Pels, F. Kapteijn, J.A. Moulijn, Q. Zhu, K.M. Thomas, Evolution of nitrogen functionalities in carbonaceous materials during pyrolysis, Carbon 33 (1995) 1641–1653.
[24] M.A. Pimenta, G. Dresselhaus, M.S. Dresselhaus, L.G. Cançado, A. Jorio, R. Saito, Studying disorder in graphite-based systems by Raman spectroscopy, Phys. Chem. Chem. Phys. 9 (2007) 1276–1290.
[25] T. Brousse, D. Bélanger, J.W. Long, To be or not to be pseudocapacitive? J. Electrochem. Soc. 162 (2015) A5185–A5189.
[26] D. Deng, X. Pan, L. Yu, Y. Cui, Y. Jiang, J. Qi, W.-X. Li, Q. Fu, X. Ma, Q. Xue, Toward N-doped graphene via solvothermal synthesis, Chem. Mater. 23 (2011) 1188–1193.
[27] R. Liu, J. Duay, T. Lane, S.B. Lee, Synthesis and characterization of RuO_2/poly (3, 4-ethylenedioxythiophene) composite nanotubes for supercapacitors, Phys. Chem. Chem. Phys. 12 (2010) 4309–4316.
[28] J. Xu, K. Wang, S.-Z. Zu, B.-H. Han, Z. Wei, Hierarchical nanocomposites of polyaniline nanowire arrays on graphene oxide sheets with synergistic effect for energy storage, ACS Nano 4 (2010) 5019–5026.
[29] X. Li, H. Wang, J.T. Robinson, H. Sanchez, G. Diankov, H. Dai, Simultaneous nitrogen doping and reduction of graphene oxide, J. Am. Chem. Soc. 131 (2009) 15939–15944.
[30] G. Ali, A. Mehmood, H.Y. Ha, J. Kim, K.Y. Chung, Reduced graphene oxide as a stable and high-capacity cathode material for Na-ion batteries, Sci. Rep. 7 (2017) 40910.
[31] S. Roldán, M. Granda, R. Menéndez, R. Santamaría, C. Blanco, Mechanisms of energy storage in carbon-based supercapacitors modified with a quinoid redox-active electrolyte, J. Phys. Chem. C 115 (2011) 17606–17611.
[32] A. Laheäär, P. Przygocki, Q. Abbas, F. Béguin, Appropriate methods for evaluating the efficiency and capacitive behavior of different types of supercapacitors, Electrochem. Commun. 60 (2015) 21–25.
[33] Q. Abbas, F. Béguin, Influence of the iodide/iodine redox system on the self-discharge of AC/AC electrochemical capacitors in salt aqueous electrolyte, Prog. Nat. Sci.: Mater. Int. 25 (2015) 622–630.
[34] E. Frackowiak, M. Meller, J. Menzel, D. Gastol, K. Fic, Redox-active electrolyte for supercapacitor application, Faraday Discuss. 172 (2014) 179–198.
[35] A.D. Awtrey, R.E. Connick, The absorption spectra of I_2, I_3^-, I^-, IO_3^-, $S_4O_6^=$ and $S_2O_3^=$. Heat of the reaction $I_3^- = I_2 + I^-$, J. Am. Chem. Soc. 73 (1951) 1842–1843.